

Detecting highly dispersed bursts with next-generation radio telescopes

T. E. Hassall,¹★ E. F. Keane^{2,3} and R. P. Fender¹

¹*School of Physics and Astronomy, University of Southampton, Southampton SO17 1BJ, UK*

²*Jodrell Bank Centre for Astrophysics, School of Physics and Astronomy, The University of Manchester, Manchester M13 9PL, UK*

³*Centre for Astrophysics and Supercomputing, Swinburne University of Technology, PO Box 218, Hawthorn, VIC 3122, Australia*

Accepted 2013 August 19. Received 2013 August 15; in original form 2013 June 12

ABSTRACT

Recently, there have been reports of six bright, dispersed bursts of coherent radio emission found in pulsar surveys with the Parkes Multibeam Receiver. Not much is known about the progenitors of these bursts, but they are highly energetic, and probably of extragalactic origin. Their properties suggest extreme environments and interesting physics, but in order to understand and study these events, more examples need to be found. Fortunately, the recent boom in radio astronomy means many ‘next-generation’ radio telescopes are set to begin observing in the near future. In this paper we discuss the prospects of detecting short extragalactic bursts, in both beamformed and imaging data, using these instruments. We find that often the volume of space probed by radio surveys of fast transients is limited by the dispersion measure of the source, rather than its physical distance (although the two quantities are related). This effect is larger for low-frequency telescopes, where propagation effects are more prominent, but their larger fields-of-view are often enough to compensate for this. Our simulations suggest that the low-frequency component of Square Kilometre Array Phase 1 could find an extragalactic burst every hour. We also show that if the sensitivity of the telescope is above a certain threshold, imaging surveys may prove more fruitful than beamformed surveys in finding these sorts of transients.

Key words: scattering – methods: observational – surveys – intergalactic medium – galaxies: ISM.

1 INTRODUCTION

Fast radio bursts (FRBs) are amongst the most violent and energetic events in the Universe. To date, there have been six bright, highly dispersed bursts found in beamformed surveys for fast transients (Lorimer et al. 2007; Keane et al. 2011; Thornton et al. 2013). The progenitors of the bursts are unknown, but the limited data that we have on them point towards extreme environments and interesting physics. Their dispersion measures (DMs) indicate that they are likely to be from outside of our Galaxy, and probably at cosmological distances (their inferred redshifts are $z \sim 0.1$ – 0.9). Although their exact distances (D) and intrinsic pulse widths (τ_0) are not well constrained, all of the bursts are known to be highly energetic, coherent emitters – FRB 010724 had a brightness temperature $\sim 10^{34} \left(\frac{D}{500 \text{ Mpc}}\right)^2 \left(\frac{\tau_0}{5 \text{ ms}}\right)^{-2}$ K and released $\sim 10^{33} \left(\frac{D}{500 \text{ Mpc}}\right)^2 \left(\frac{\tau_0}{5 \text{ ms}}\right)$ J of energy. Light travel time arguments show that the bursts must originate from compact regions (with upper limits on the diameters ranging from 300 to 1500 km). Keane et al. (2012) argued that FRB 010621 could potentially be explained as an annihilating mini black hole or a ‘giant pulse’ from a young pulsar with a low burst

rate, but only if the NE2001 model of the Galactic electron density (Cordes & Lazio 2002) is sufficiently incorrect as to allow the burst to originate from inside our Galaxy. They found no consistent explanation for FRB 010724, although Lorimer et al. (2007) noted that the implied rate of occurrence is compatible with that of gamma-ray bursts.

As well as being interesting in their own right, these objects are also potentially powerful tools for studying the intergalactic medium (IGM). They vary on very short time-scales, allowing us to measure the dispersive delay and scatter broadening time-scale, which can be used to determine the density and spatial distribution of electrons along the line of sight. They may also prove useful for cosmological measurements if the bursts are standard, or ‘standardizable’, (Phillips 1993) candles.

In order to study and understand this population of objects, it will be necessary to find many more of them. All of the known bursts have been found through ‘pulsar-like’ beamformed observations at relatively high frequencies (~ 1.4 GHz), but, because FRBs are so bright, they may also be detectable in images. Note, in this paper we choose to use ‘beamformed’ to describe pulsar-like observations, even though in some cases beams are not formed digitally. Beamformed surveys have been successful in the past, and they are known to be sensitive to these bursts and to other bright single pulses

★E-mail: t.hassall@soton.ac.uk

(e.g. rotating radio transients, ‘RRATs’; Keane & McLaughlin 2011). However, the localization of the sources is relatively poor, and in some cases, it can be difficult to distinguish real pulses from radio frequency interference (RFI; see Burke-Spolaor et al. 2011). Imaging surveys could (in some circumstances) offer a better localization of the source, and are also potentially more robust against RFI, but because the bursts are so rapid and radio images have a practical limit on their shortest exposures, some of the sensitivity of the survey may be lost. In this paper, we compare the number of simulated FRBs detected in imaging and beamformed surveys with several ‘next-generation’ radio telescopes. We also investigate the effects of dispersion and scattering on the bursts and determine the most effective observatories for locating such events.

2 PROPAGATION EFFECTS

As pulsed emission passes through an ionized plasma it interacts with electrons along the line of sight, and becomes distorted by dispersion and scattering. The peak flux of a pulse is reduced, and the emission becomes smeared out in time, making it more difficult to detect. Although propagation effects are particularly prominent at low frequencies, they need to be considered at all frequencies when trying to determine the rate of short bursts. In the following section we summarize the two propagation effects we consider here.

2.1 Dispersion

The frequency-dependent refractive index of a cold, ionized plasma means that any signals propagating through it are dispersed. Emission at frequency, ν (in MHz), is delayed with respect to emission at infinite frequency by, Δt_{DM} (in s),

$$\Delta t_{\text{DM}} = \frac{\text{DM}}{2.410 \times 10^{-4} \nu^2}, \quad (1)$$

where DM is the dispersion measure in units of pc cm^{-3} . In beamformed analysis, this delay can be addressed either by channelizing the data and compensating for the delay in each channel, significantly reducing the effects of dispersion across the band (‘incoherent dedispersion’; Large & Vaughan 1971), or applying a frequency-dependent delay to the raw voltage data directly and completely removing the dispersive delay (‘coherent dedispersion’; Hankins & Rickett 1975). Coherent dedispersion is the more precise method, but typically incoherent dedispersion is used in blind searches for pulsars and fast transients, as coherent dedispersion is usually too computationally expensive.

Whilst dedispersion makes searching for new objects more difficult, once the correct DM of a source is known, it can be removed. Dispersion also provides a good way to discriminate between a real signal and RFI, as terrestrial signals do not typically follow a ν^{-2} law. The fact that all of the previously reported bursts follow the dispersion law so well, remains the strongest evidence that they are of astrophysical origin. As the dispersive delay depends only on the number of electrons along the line of sight, and not their distribution, the dispersive delay will follow the same ν^{-2} law in both the interstellar medium (ISM) and the IGM. However, the relation between the DM and the column density of electrons of redshifted sources will be different from that predicted theoretically and observed for Galactic sources (see Ioka 2003, for a more detailed discussion).

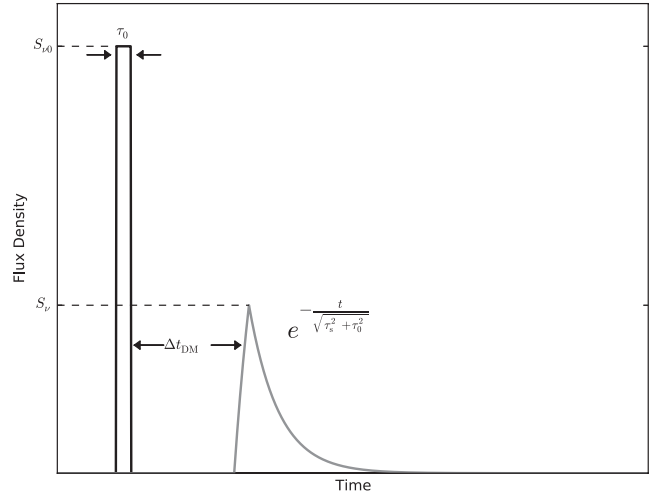


Figure 1. A boxcar pulse with initial pulse density S_{v0} (black line) is scatter broadened by the ISM. Its peak flux density is reduced to S_v and its profile changes (grey line), increasing the pulse width to $\sim \sqrt{\tau_0^2 + \tau_s^2}$.

2.2 Scattering

As radio waves propagate through a plasma, they are also scattered by fluctuations in the electron density along the line of sight. This results in multipath propagation, which temporally broadens narrow pulses. In the simplest case of a scattering screen located midway between the source and observer this effectively convolves the narrow pulse with a one-sided exponential with scattering time-scale, τ_s ¹ (see Fig. 1). Detailed reviews of interstellar scattering can be found in Rickett (1990) and Narayan (1992).

The scatter-broadening time of a pulsed signal passing through the ISM is related to the DM by the empirical function derived by Bhat et al. (2004),

$$\log \tau_s = 2.12 + 0.154 \log(\text{DM}) + 1.07(\log \text{DM})^2 - 3.86 \log \nu, \quad (2)$$

where ν is the observing frequency in MHz, and τ_s is the scatter broadening time in s. Although, it should be noted that observed values of τ_s for a given DM can deviate from the predicted value by up to two orders of magnitude and the frequency dependence of τ_s depends strongly on the distribution of the electron density along the line of sight.

As the peak flux is typically used as the detection threshold it is important we address how it is affected by scattering. When a pulse is scattered, it is smeared out over a longer time, reducing the peak flux density. If we assume that the unscattered pulse is a step function with intrinsic width τ_0 , and a peak flux density of S_{v0} , then its intrinsic fluence is $\mathcal{F} = S_{v0} \tau_0$. As the pulse is broadened by scattering, the fluence at a given frequency, F_v , is given by

$$F_v = S_v \sqrt{\tau_0^2 + \left(\int_0^\infty e^{-t/\tau_s} dt \right)^2} = S_v \sqrt{\tau_0^2 + \tau_s^2}, \quad (3)$$

where S_v is the observed peak flux density at frequency ν . If we assume that the fluence is conserved by scattering (i.e. any emission

¹ Multipath propagation also blurs the pulses spatially, increasing the observed angular size of the source by $\theta_s \sim \sqrt{\frac{4.8c}{D}}$. We do not consider this effect here, however, because the distance to the source is typically large. To blur a source 1 kpc away by 10 arcsec, $\tau_s \sim 250$ s.

Table 1. Observed properties of known extragalactic bursts.

	FRB 010724	FRB 010621	FRB 110220	FRB 110627	FRB 110703	FRB 120127
Observed width (ms)	4.6	8.3	5.6	<1.4	<4.3	<1.1
$(\tau_0^2 + \tau_s^2)^{1/2}$ (ms)	3.1	4.8	5.5	<1.1	<4.1	<0.9
Predicted τ_s (ms) ^a	2.89	177	802	145	2251	28
DM (pc cm ⁻³)	375 ± 1	746 ± 1	944.38 ± 0.05	723.0 ± 0.3	1103.6 ± 0.7	553.3 ± 0.3
Extragalactic DM (pc cm ⁻³)	330	213	910	677	1072	521
Peak flux density (Jy)	30 ± 10	0.4 ± 0.1	1.3	0.4	0.5	0.5
Spectral index ^{b2}	-4 ± 1	0 ± 1	0 ± 1	0 ± 1	0 ± 1	0 ± 1
Observed rate (h ⁻¹ deg ⁻²) ^c	0.0019 ^{+0.0045} _{-0.0006}	0.00051 ^{+0.0013} _{-0.0001}	0.0017 ^{+0.0013} _{-0.0005}	0.0017 ^{+0.0013} _{-0.0005}	0.0017 ^{+0.0013} _{-0.0005}	0.0017 ^{+0.0013} _{-0.0005}

^aFrom Bhat et al. (2004).

^bSpectral index of the peak flux density.

^cUncertainties are determined following Gehrels (1986).

scattered out of the line of sight is balanced by emission scattered into it), then the peak flux is given by

$$S_\nu = \frac{\mathcal{F}}{\sqrt{\tau_0^2 + \tau_s^2}}. \quad (4)$$

At high frequencies (or low DMs), where $\tau_0 \gg \tau_s$, the peak flux is approximately constant, but when $\tau_s \gtrsim \tau_0$, scattering causes the peak flux to decrease as $S_\nu \propto 1/\tau_s$ ($\propto \nu^{3.86}$, if the scatter broadening follows equation (3)). At low observing frequencies (or high DMs), the temporal pulse broadening is large, and there is a significant reduction in peak flux.

Scatter broadening of extragalactic sources has only been observed twice (Thornton et al. 2013), and is therefore not well understood, but current observations suggest that it is probably quite different from the scattering seen from the ISM. It has not yet been possible to measure the distribution of electrons in the IGM, but one possibility is that the density fluctuations are less significant than those seen in the ISM. The so-called ‘lever-arm’ effect is also expected to reduce scatter broadening; the observed effect is maximized when scattering material is concentrated halfway between the observer and the source. So, because most of the scattering material will be concentrated in the ISM of our Galaxy and the host galaxy, the scatter broadening of extragalactic sources may be reduced (Lorimer et al. 2013). This is consistent with the findings of the two known FRBs, which, despite having large DMs, showed very little scatter broadening (in many cases, significantly less than what was expected from Bhat et al. 2004, see Table 1).

2.3 Propagation effects in known FRBs

We find it appropriate here to compare the properties of the previously reported bursts. The relation between the observed width, W , and the intrinsic width, τ_0 , can be written as

$$W^2 = \tau_0^2 + \tau_{\text{DM}}^2 + \tau_s^2 + \tau_{\text{samp}}^2, \quad (5)$$

where τ_{DM} is the dispersive delay across a single channel; for a frequency resolution $\Delta\nu$, an observing frequency of ν and a DM, the dispersive smearing is $\tau_{\text{DM}} = 4.5(\text{DM}/500 \text{ cm}^{-3} \text{ pc})(\Delta\nu/3 \text{ MHz})(1400 \text{ MHz}/\nu)^3 \text{ ms}$; τ_s is the unknown scattering time and τ_{samp} is the sampling time of the observation. Unless the pulse is completely resolved, and the scatter broadening can be measured (as for FRB 110220; see Thornton et al. 2013), the extent of the scatter broadening is unknown and we can only place an upper limit on the intrinsic pulse width of any detected signal.

FRB 010724 (010621) had an observed pulse width of 4.6 ms (8.3 ms) at an observational frequency of 1400 MHz. Removing the

dispersive smearing gives $(\tau_0^2 + \tau_s^2)^{1/2}$, i.e. an upper limit on the intrinsic width (at 1400 MHz), of 3.1 ms (4.8 ms), with a corresponding upper limit on the size of the source of $\sim 900 \text{ km}$ ($\sim 1400 \text{ km}$) which is much smaller than the minimum allowed radius of a white dwarf. Similarly, the FRBs found by Thornton et al. (2013) also seem to have narrow intrinsic pulse widths, the only pulses with $W > 2 \text{ ms}$ seem to have been scatter broadened. In what follows we consider intrinsic pulse widths of 1 ms. All FRBs have DM values in excess of the maximum expected contribution from the Galaxy along their respective lines of sight. This places them outside the Galaxy, and using the model of Ioka (2003) we can infer redshifts between $z \sim 0.1$ and ~ 0.9 for the sources. Using a cosmological model [e.g. Λ cold dark matter (Λ CDM)] we can infer a distance and thence a luminosity. This line of reasoning leads to the conclusion that the bursts are very bright, ~ 12 orders of magnitude more luminous than the typical pulses seen from pulsars, and ~ 6 orders of magnitude more luminous than the brightest pulse ever observed from the Crab pulsar (see fig. 1 of Keane et al. 2011). We note that the dependence on frequency of the flux density and the pulse width is seen to be quite steep for FRB 010724 but very flat for FRB 010621 (although if either of the bursts was detected away from the centre of the telescope beam, the spectral index would appear steeper than it actually is). The spectral indices of the bursts from Thornton et al. (2013) were all consistent with being flat. In our simulations below we consider a wide range of spectral indices² and show the results for all cases. Some properties of the bursts are summarized in Table 1.

3 RATE CALCULATIONS

3.1 Determining rates of FRBs

As there are only six known FRBs, it has so far been impossible to properly determine the luminosity function of the bursts. So, for the purposes of this paper, we will assume that the bursts are standard candles, which emit over all frequencies following a constant spectral index. It then follows that the number of events which will be seen in a given observation (N_{obs}) is given by

$$N_{\text{obs}} = \rho_0 t_{\text{obs}} V_{\text{obs}}, \quad (6)$$

where ρ_0 is the rate at which the events occur per unit time per unit volume, t_{obs} is the total amount of observing time and V_{obs} is the volume of extragalactic space being probed in the observations. We

²In this paper, we follow the convention of defining the spectral index α as $S_\nu \propto \nu^\alpha$.

note that, as FRBs are at cosmological distances, the comoving volume must be used for this calculation. For a given instrument, which is sensitive to bursts above a given luminosity out to a comoving radial distance of D_{\max} and has a beam shape B , this is given by

$$V_{\text{obs}} = \int_{\phi=0}^{2\pi} \int_{\theta=0}^{\pi} \int_{r=0}^{D_{\max}} B r^2 \sin \theta \, dr \, d\theta \, d\phi. \quad (7)$$

Generally the beam shape will not depend on r , so we can rewrite the equation as

$$V_{\text{obs}} = \frac{1}{3} D_{\max}^3 \int_{\phi=0}^{2\pi} \int_{\theta=0}^{\pi} B(\theta, \phi) \sin \theta \, d\theta \, d\phi = \frac{\Omega}{3} D_{\max}^3, \quad (8)$$

where Ω is the integrated surface area of the beam shape in steradians.³ Typically, in the local Universe, D_{\max} varies as $S_{\min}^{-1/2}$ (the minimum detectable flux density) which, combined with equations (6) and (8), gives rise to the well-known $N \propto S^{-3/2}$ relation.

In radio surveys for ‘fast’ transients, however, propagation effects are important. Dispersion delays the pulse with decreasing frequency and scattering broadens the pulse, reducing its peak flux. This means that D_{\max} may be limited by the dispersion and scatter broadening along the line of sight rather than the luminosity and distance to the source. A significant contribution to the DM of extragalactic bursts comes from our Galaxy⁴ (and any putative host galaxy). Because it reduces the peak flux of the signal, this component of the DM effectively reduces the observable volume of the Universe. The rest of the DM comes from the IGM. This intergalactic DM (DM_{IGM} , in pc cm^{-3}) may be related to the redshift of the source (Ioka 2003):

$$z \approx \frac{\text{DM}_{\text{IGM}}}{1000}. \quad (9)$$

Note, the value DM_{IGM} given by Ioka accounts for the fact that the observed emission has been cosmologically redshifted. This redshift can be converted into a comoving radial distance using COSMOCALC (Wright 2006), with the cosmological constants derived from the latest *Planck* results ($H_0 = 68 \text{ km s}^{-1}$, $\Omega_M = 0.32$, $\Omega_\Lambda = 0.68$; Ade et al. 2013).

The dispersion and scattering in the ISM and the IGM mean that, in radio surveys, the flux density of dispersed transients will appear to drop more quickly with distance than expected from the inverse-square law. There is an additional effect which needs to be considered which arises because the optimal signal-to-noise ratio (SNR) of a given data set is achieved when the binning time of the data is approximately equal to the pulse width. If this time is too short, then not all of the pulse is observed, and if it is too long then unnecessary noise is added to the signal, effectively increasing the minimum flux we are sensitive to (and therefore reducing the observed volume). The combination of the luminosity, distance, propagation effects and binning time makes D_{\max} difficult to determine analytically, so we use simulations to determine the rate of FRBs, and the volume of the Universe sampled by several next-generation observatories.

³ $\Omega \approx a^2$ if we assume the beam is a square step function, and $\Omega \approx 2\pi a^2$ for a circularly symmetrical Gaussian beam with (small) angular width a . More complex beam patterns [e.g. that of Low Frequency Array (LOFAR)] are most easily determined by integrating the beam shape numerically.

⁴ The maximum Galactic DM ranges from ~ 20 to 2000 pc cm^{-3} depending on the line of sight (Cordes & Lazio 2002).

3.2 Simulations

We simulated pulses (with 1 ms intrinsic width, assumed to be standard candles with the mean specific luminosity of the six known bursts; 50 Jy Gpc^2 at 1400 MHz)⁵ propagating through space, and interacting with the ISM and IGM, then being observed with a range of integration/binning times. For our calculations, we assume that the fluence of the pulse is conserved through scattering; if this is not the case, the sensitivity to scattered FRBs will be reduced. Binning times for beamformed observations were limited to $0.001 < t_{\text{bin}} < 0.1 \text{ s}$, and the integration times for images were chosen to be $1 < t_{\text{int}} < 10\,000 \text{ s}$. The lower limit of 1 s for imaging surveys was arbitrarily chosen to distinguish between imaging and beamformed observations. If images are taken on shorter time-scales, then the imaging rates will improve because they will be more sensitive to unscattered FRBs. The dwell times for the simulated observations were chosen to be 600 s for beamformed observations, and 10 000 s for imaging observations. Care should be taken when selecting a dwell time for FRB observations to ensure the dwell time is significantly longer than the dispersive delay across the band, so the probability of detecting the whole dispersed pulse (and hence the sensitivity of the observation) is maximized. We assume that beamformed data are perfectly dedispersed, and images are not dedispersed at all. The simulations are performed for DMs from 0 to 6000 pc cm^{-3} ($z \sim 0-6$, where $z \sim 6$ corresponds to the end of cosmic reionization in Ioka’s simulations). For beamformed observations, we assume that the entire field-of-view can be tiled out with coherently combined beams, which have the same sensitivity as imaging observations. Noise levels were based on expected values for the effective area and system temperature of operating and planned telescopes from the scientific literature and scaled assuming the integrated noise $\propto \sqrt{t_{\text{int}}}$ (see Table 3 for the specific parameters used to simulate each observatory).

The electron distribution in the IGM is not well known, but because the concentration of electrons is thought to be lower in the IGM, we anticipate that the scatter broadening of pulses by the IGM may be lower than that of our Galaxy. Any contribution to the DM or scatter broadening from a host galaxy will also be reduced because it will be redshifted from higher frequencies. We therefore simulated two scenarios.

- (i) *High scattering*. The IGM causes temporal scatter broadening which follows the Bhat et al. (2004) relation (the same as the ISM).
- (ii) *No scattering*. There is no temporal scatter broadening.

The real rate will lie between these two extremes. Where not specified, the Galactic DM is assumed to be 150 pc cm^{-3} , which is the mean DM of all directions in the sky (based on the NE2001 model; Cordes & Lazio 2002).

3.3 Rate of the Parkes FRBs

We calculate ρ_0 by applying our simulations to the surveys which found the known FRBs. The surveys concerned are the Parkes Magellanic Clouds Pulsar Survey (MCPS; Manchester et al. 2006), the Parkes Multibeam Pulsar Survey (PMPS; Manchester et al. 2001) and the High Time Resolution Universe Survey (HTRU; Keith et al. 2010). All surveys were undertaken using the Parkes Multibeam Receiver (see Table 3 for instrumental properties). The MCPS observed for a total of 480 h, the PMPS observed for a

⁵ This specific luminosity, if persisting over 20 GHz, corresponds to a radio-band luminosity of $\sim 10^{37} \text{ W}$ and an energy release of $10^{34} \text{ (W/1 ms) J}$.

total of 1800 h and at the time of the publication of Thornton et al. (2013), 552 h of the HTRU had been searched for FRBs. One FRB was found in the MCPS and the PMPS, and four were found in 24 per cent of the HTRU. We used our simulations to determine the volume of sky covered in each survey, and then used that to determine ρ_0 .

We find that in both of the proposed scattering scenarios, the MCPS was limited by the maximum value of DM the data were dedispersed to, the DM range used was 0–500 pc cm⁻³ (~ 75 pc cm⁻³ of which was Galactic), the survey was sensitive to $D_{\max} \sim 1.9$ Gpc. The field-of-view used in our simulations is significantly lower than that of Lorimer et al. (2007), which we feel was overestimated. The half-power beamwidth of a single beam of the Parkes Multi-beam receiver is ~ 14 arcmin (Staveley-Smith et al. 1995), thus the integrated surface area of a Gaussian function approximating a single beam is ~ 0.086 deg², and the field-of-view of the full, 13-beam receiver is ~ 1.1 deg². This leads to a slightly higher estimate of the event rate, $\rho_0 = 98^{+225}_{-78}$ Gpc⁻³ d⁻¹. In the high-scattering simulations, the PMPS was limited by scatter broadening, and was sensitive out to $D_{\max} \sim 2.5$ Gpc, giving a rate of 12^{+27}_{-9} Gpc⁻³ d⁻¹. In the no-scattering simulations, the PMPS was limited by the DM range searched, 0–2200 pc cm⁻³ (~ 250 pc cm⁻³ of which was Galactic), $D_{\max} \sim 5.5$ Gpc, yielding a significantly lower value for the event rate, $\rho_0 = 1.1^{+2.5}_{-0.9}$ Gpc⁻³ d⁻¹. Note that the agreement between the rates from the two surveys is significantly reduced when the IGM does not scatter broaden the pulses, although the rates are roughly compatible in both cases. The HTRU was also limited by scatter broadening in the high-scattering simulations ($D_{\max} \sim 2.5$ Gpc, $\rho_0 \sim 143^{+114}_{-42}$ Gpc⁻³ d⁻¹), and by the DM range searched in the no-scattering simulations ($D_{\max} \sim 5.2$ Gpc, $\rho_0 \sim 17^{+13}_{-5}$ Gpc⁻³ d⁻¹). The rates derived from the HTRU are more compatible with the rates from the MCPS than the PMPS. The reason for this may be because most of the observations from the PMPS were in directions closer to the Galactic plane, where local scatter broadening and dispersion are strongest. Thus, the true event rate may be closer to the high-scattering simulations for the PMPS, and the no-scattering simulations in the MCPS and HTRU observations.

To find the combined rate of all of the Parkes surveys, we multiplied the Poissonian distributions implied from the calculated rates together, and found $\rho_0 = 51^{+31}_{-14}$ Gpc⁻³ d⁻¹ for the high-scattering simulations and $5.3^{+3.1}_{-1.4}$ Gpc⁻³ d⁻¹ for the no-scattering simulations. These are the values we use in all subsequent simulations. The true event rate lies somewhere between these two values, and from the observational evidence of the six known bursts, probably closer to the no-scattering simulations. So (as was discussed in Lorimer et al. 2007) this is compatible with rates for short GRBs and neutron star inspirals, but significantly lower than the rate of core-collapse supernovae unless the bursts are beamed (see Table 2). We note that

Table 2. Comparison of transient rates.

Object	Rate ^a (Gpc ⁻³ d ⁻¹)	Reference
FRBs (high scattering)	51^{+31}_{-14}	This work
FRBs (no scattering)	$5.3^{+3.1}_{-1.4}$	This work
Short GRBs	$\sim 0.3\text{--}3$	Fong et al. (2012)
NS mergers	$\sim 0.3\text{--}30$	Abadie et al. (2010)
CC supernovae	$\sim 200\text{--}2000$	Li et al. (2011)

^aThe rates given here are ‘local’ ($z < 1$), but the true rates depend on redshift. They should be treated as order of magnitude estimates.

the DM range searched is the limiting factor in the no-scattering simulations for all surveys, so we predict that reprocessing the data out to a higher DM will yield new FRB detections.

3.4 Other observatories

Using the rates derived from the Parkes surveys, we applied our simulations to other existing and planned observatories to determine which will be most suitable for finding FRBs. The observatories considered, and the observing parameters used in the simulations are summarized in Table 3. We note that even if the occurrence rate changes significantly as more FRBs are discovered, the relative performance of the telescopes shown in these plots will remain accurate, and the detectable numbers will simply be scaled by a constant factor. Figs 2 and 3 show the results of the simulations for the high-scattering and no-scattering simulations, respectively, at each observatory. The coloured bars show the number of FRBs detectable in imaging surveys, assuming different spectral indices of 0.0 (white), -1.0 , -2.0 , -3.0 and -4.0 (darkest grey). The number of FRBs detectable in beamformed surveys is indicated by the bars with a solid black outline. These results are also tabulated in Appendix A.

It is clear from the figures that in the low-scattering simulations, beamformed observations are typically more efficient at finding FRBs than imaging observations, however, in telescopes which are very sensitive (e.g. SKA-mid), imaging surveys are competitive. In the high-scattering simulations, imaging surveys are often much more effective. We note that, as the amount of scatter broadening is not known a priori, both imaging *and* beamformed observations are needed to maximize chances of detection. One can also see that the field-of-view of the telescope makes a big difference. This is most obvious when comparing Australian Square Kilometre Array Pathfinder (ASKAP) and the Parkes telescope in the no-scattering beamformed simulations. Whilst both telescopes observe at similar frequencies, ASKAP is slightly less sensitive, but should find many more FRBs because of its much larger field-of-view (although this relies on the assumption that the entire field-of-view can be tiled out with coherently added beams in beamformed mode). MeerKAT also observes at the same frequency is far more sensitive, and has a much wider bandwidth, but because the field-of-view is only 1 deg², it will find FRBs at a slightly lower rate than Parkes, and at a significantly lower rate than ASKAP.

4 SEARCH STRATEGIES

4.1 Matched filtering

Matched filtering is used to maximize the SNR of a given data set. This is done by correlating noisy data with a noiseless template approximating the shape of the underlying signal being searched for. Since the shape and width of the pulse are not known a priori this is most simply done by iteratively summing adjacent samples. This technique is commonly used in single pulse searches of beamformed data (Cordes & McLaughlin 2003), and should also be applied when searching for transients in images. Images should be searched on a range of time-scales (i.e. varying integration times) in order to tune observations to pulses of different widths.

For scattered bursts, the shape of the signal at a given frequency is an exponentially decaying pulse, e^{-t/τ_s} . The integrated signal of the pulse increases as $\tau_s(1 - e^{-t_{\text{int}}/\tau_s})$, whilst the integrated noise level

Table 3. Comparison of the parameters used for simulations of current and planned telescopes. The values of field-of-view and $A_{\text{eff}}/T_{\text{sys}}$ given here are calculated for the centre of the observing band listed. For LOFAR, we use noise levels derived from current transient imaging surveys, which may improve in the future.

Telescope	$A_{\text{eff}}/T_{\text{sys}}$ (m^2/K)	ν_{low} (MHz)	ν_{high} (MHz)	FoV (deg^2)	Reference
SKA-low	5000	50	350	27	Dewdney et al. (2013)
SKA ₁ -low	1000	50	350	27	Dewdney et al. (2013)
SKA-mid	10 000	1000	2000	0.5	Dewdney et al. (2013)
SKA ₁ -mid	1630	1000	2000	0.5	Dewdney et al. (2013)
LOFAR-HBA	110	155	165	150	Stappers et al. (2011), van Haarlem et al. (2013)
LOFAR-LBA	0.5	30	80	100	Stappers et al. (2011), van Haarlem et al. (2013)
MWA	13.0	185	215	375	Tingay et al. (2013)
ASKAP	81	700	1000	30	Johnston, Feain & Gupta (2009)
MeerKAT	220	580	1750	1.0	de Blok et al. (2010)
Parkes Multi-beam	92	1230	1518	1.1	Manchester et al. (2001)
Molonglo	277	790	890	12	Green et al. (2012)
UTR-2	0.5	10	20	40	Abranin et al. (2001)
LWA	30	50	70	20	Ellingson et al. (2009)

increases as $\sqrt{t_{\text{int}}}$. Therefore, the SNR as a function of integration time, t_{int} , scales as

$$\text{SNR} \propto \frac{\tau_s(1 - e^{-t_{\text{int}}/\tau_s})}{\sqrt{t_{\text{int}}}}, \quad (10)$$

the peak of this function occurs when $t_{\text{int}} \approx \tau_s$. This is complicated by the frequency evolution of the pulse, but from our simulations, we find that generally, as adding noise only reduces sensitivity by $1/\sqrt{t_{\text{int}}}$, the optimum integration time is approximately equal to the scatter-broadening time at the bottom of the band. Using a range of integration times makes the data sensitive to pulses of different durations. This part of the search process is particularly important for low-frequency surveys, where scatter broadening means that pulse widths can range from a few milliseconds to several hours.

4.2 Line of sight

The specific lines of sight used will have a significant impact on the sensitivity of a transient survey. Scattering significantly reduces the peak flux of a pulse, so maximal sensitivity to extragalactic sources is achieved when observing away from the Galactic plane ($|b| \gtrsim 10^\circ$), where the electron density along the line of sight, and therefore the scatter-broadening time, is lowest. This will impact all radio transient surveys, but is particularly important at low frequencies. Fig. 4 shows the number of FRBs expected to be observed per hour using the LOFAR HBAs (black lines) and ASKAP (grey lines) in our high-scattering simulations as a function of the Galactic DM along the line of sight (see Table 3 for the specifications of the telescopes used in the simulation). The contribution from the host galaxy is assumed to be small, but we do consider the contribution from the IGM. The solid lines show the rates for imaging observations, and the dashed lines show the rates for beamformed observations. For LOFAR beamformed observations, choosing a ‘clear’ line of sight can improve the chances of detecting an FRB by a factor of $\sim 10^4$. For ASKAP (a higher frequency instrument), the effect is smaller, but still makes a significant difference. The effect is less pronounced in imaging observations, but still important. It should be noted that the simulations used to produce Fig. 4 do not include the lever-arm effect, and because this will reduce scatter broadening, the trend may be slightly exaggerated. However, even in the no-scattering simulations, choosing a line of sight with a

low Galactic DM still increases the volume of extragalactic space probed.

4.3 Dedispersion

Dedispersion is only beneficial for detecting FRBs when the dispersive delay across the band (Δt_{DM}) is larger than the observed width of the pulse (W). Fig. 5 shows $\Delta t_{\text{DM}}/W$ as a function of DM for a pulse detected at a central frequency of 1500 MHz with 1000 MHz bandwidth in the high-scattering simulations. At low DMs, W is dominated by the intrinsic width of the pulse and it is not necessary to dedisperse the data because Δt_{DM} is small. Δt_{DM} increases with DM until it exceeds the intrinsic pulse width, at which point dedispersion becomes necessary. This is the regime which FRBs (and pulsars) are normally detected in beamformed surveys. However, above a certain DM, the scatter broadening of the pulse, which increases more rapidly with DM than the dispersive delay, means that W eventually exceeds Δt_{DM} again. Thus, for highly scattered sources, it is not beneficial to dedisperse the data. It is these highly scattered objects which would be the targets of imaging surveys for FRBs. At low frequencies, or with narrower bandwidths, the critical DM at which scatter broadening exceeds Δt_{DM} is shifted to lower DMs. For example, using the maximum bandwidth available with the LOFAR high band antennas (96 MHz), with a central frequency of 150 MHz, the SNR of observations is not improved by dedispersion for DMs above $\sim 400 \text{ pc cm}^{-3}$. For the LOFAR low band antennas (80 MHz bandwidth, centred on 60 MHz), dedispersion does not enhance our sensitivity for DMs above $\sim 250 \text{ pc cm}^{-3}$. The bursts we are interested in occur outside our Galaxy, which means they typically have DMs $> 150 \text{ pc cm}^{-3}$ from the Galactic dispersion along the line of sight, and the dispersion from within their host galaxy. So, although LOFAR imaging observations will not be dedispersed, that should not impact their chances of detecting such bursts significantly.

4.4 Imaging versus beamformed observations

Imaging surveys are competitive with beamformed surveys in finding FRBs when the scattering of the pulse is significant. This is because images are inherently more robust against RFI (affected stations can be removed and spurious sources can be rejected when they do not appear point-like, although with better RFI-removal

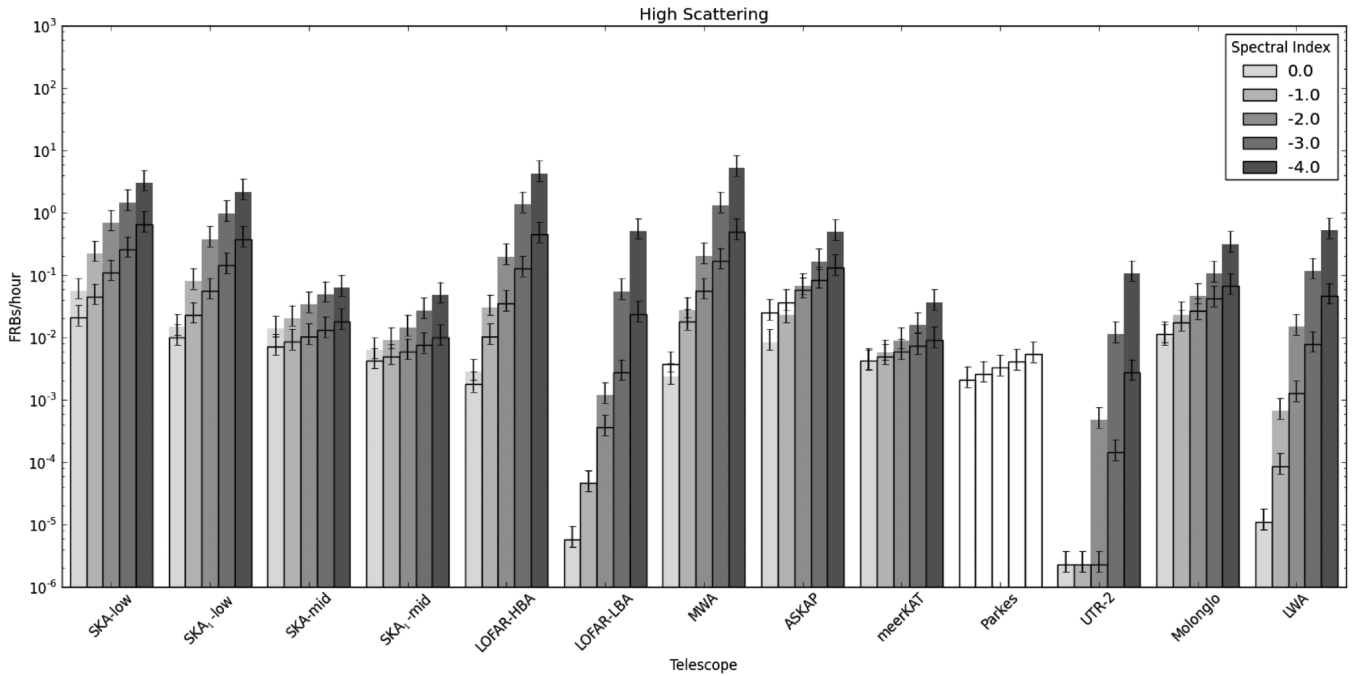


Figure 2. Expected number of FRBs per hour for various observatories in the high-scattering simulations. The coloured bars show the number of FRBs detectable in imaging surveys, assuming different spectral indices of 0.0 (white), -1.0 , -2.0 , -3.0 and -4.0 (darkest grey). The number of FRBs detectable in beamformed surveys is indicated by the bars with a solid black outline. The DM range used was $0\text{--}6000\text{ pc cm}^{-3}$.

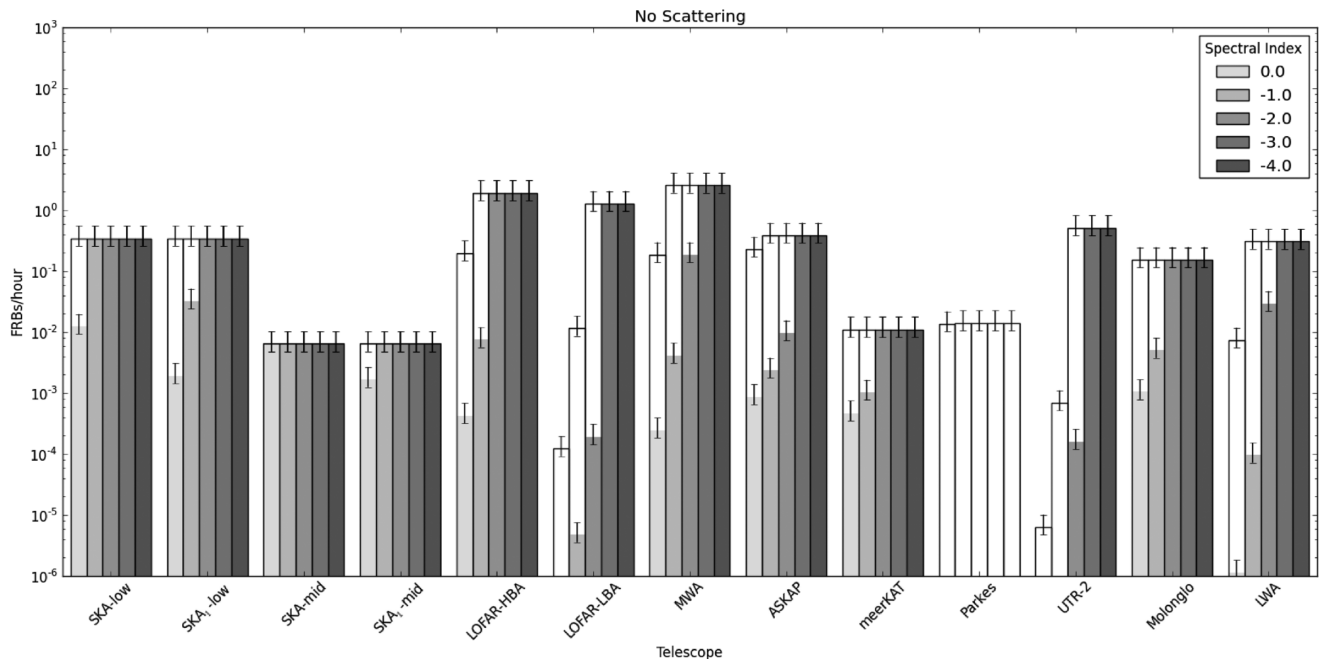


Figure 3. As Fig. 2, but for the no-scattering simulations.

algorithms the difference between imaging and beamformed data could be reduced), and more stable on long time-scales. In addition, because the more distant elements of an array are easier to include in imaging observations, finding FRBs in images could offer a much better localization of the source, and could help to associate it with a host galaxy. Unfortunately, producing images which have integration times shorter than a few minutes is often difficult because short integrations have reduced UV coverage, which can lead to

difficulties calibrating and cleaning the data correctly. Exceptions to this include arrays with good instantaneous UV coverage, and situations where the burst dominates the flux in the field-of-view. Also, there is a practical limit on the shortest images, which is set by the shortest possible correlator time, so images are less sensitive to short bursts, and may be unable to resolve scatter broadening or dispersion (although this limit has been improved radically; see Law et al. 2011).

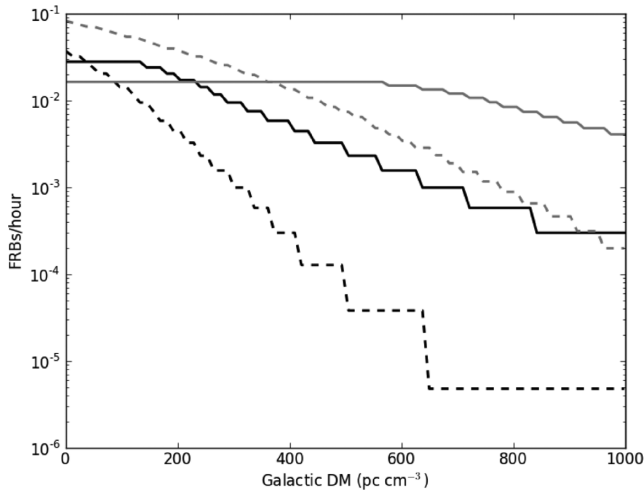


Figure 4. The number of detectable FRBs per hour as seen by the LOFAR HBAs (black lines) and ASKAP (grey lines). The solid lines correspond to imaging observations, and the dashed lines correspond to beamformed observations. The spectral index used for these simulations is $\alpha = -2.0$, but changing the spectral index only affects the scale of the figure, and does not impact shape of the curves significantly. The observing parameters of both observatories are given in Table 3.

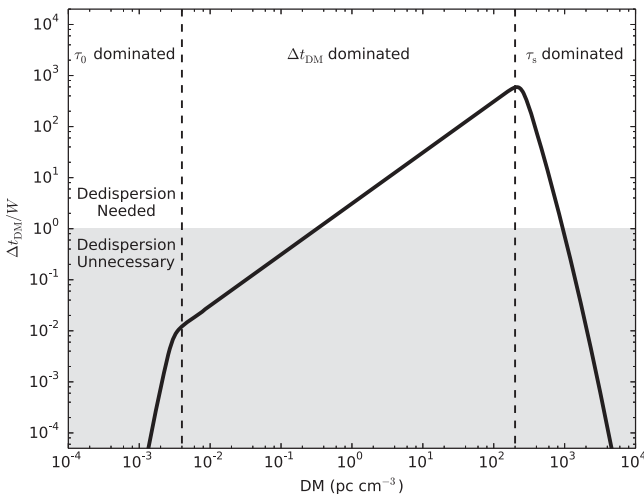


Figure 5. $\Delta t_{DM}/W$ plotted as a function of DM for a pulse detected at a central frequency of 1500 MHz with 1000 MHz bandwidth in the high-scattering regime. Dedispersion is necessary when $\Delta t_{DM}/W > 1$ (the white area of the plot), but becomes unnecessary when $\Delta t_{DM}/W < 1$ (the grey area of the plot).

This means that imaging observations are not as efficient as beamformed observations for short-duration pulses. In addition, dedispersion significantly increases the SNR for short pulses, and becomes vital when scatter broadening is small. Because of the amount of extra processing required, this is impractical on imaging data sets but is easily manageable on beamformed data, which tend to have much lower data rates. When scatter broadening is important, however, imaging observations are much more robust. It is easy to introduce long-time-scale fluctuations into the baselines of beamformed data, which reduce the sensitivity to very scattered bursts. For example, with LOFAR, bright sources moving in and out of the sidelobes of the beam can cause the baseline to fluctuate on time-scales of a few minutes. Where possible, fast transient surveys should perform ob-

servations with both imaging *and* beamformed data as both modes probe different areas of pulse width parameter space.

5 CONCLUSIONS

The next generation of radio telescopes should find a large population of FRBs. In the most optimistic scenario, the low-frequency component of SKA₁ could find up to 1 FRB per hour. However, FRB searches must be optimized, in order to increase the probability of detection. The instantaneous field-of-view should be as large as possible, FRBs are bright and do not require much sensitivity to detect, but they are quite rare, so probing a large volume of space is beneficial. This volume can in some circumstances be limited by the range of DMs searched, so processing to very high DMs (e.g. up to at least 6000) will maximize new discoveries. The line of sight through the Galaxy should be chosen carefully to minimize any local contribution to scattering and dispersion. Finally, matched filtering should be employed in both imaging and beamformed surveys of transients – the sampling time should be matched to the duration of the bursts to maximize detection. In the case of typical imaging surveys, this means that the data should be imaged on a range of time-scales from seconds to hours. Imaging surveys for FRBs in some circumstances can be competitive with beamformed observations, and it should be possible to detect FRBs in imaging surveys for ‘slow’ transients. Any such detection would be very useful because of the potential to identify the host of the event. We also note that imaging surveys probe different pulse widths than those of beamformed surveys, and could be effective at detecting the potential population of highly scattered FRBs. As the extent of the scatter broadening is not known a priori, the most effective use of telescope time would involve simultaneous beamformed and imaging surveys.

ACKNOWLEDGEMENTS

This project was funded by European Research Council Advanced Grant 267697 ‘4 Pi Sky: Extreme Astrophysics with Revolutionary Radio Telescopes’.

REFERENCES

- Abadie J. et al., 2010, *Classical Quantum Gravity*, 27, 173001
 Abranin E. P., Bruck Y. M., Zakharenko V. V., Konovalenko A. A., 2001, *Exp. Astron.*, 11, 85
 Ade P. A. R. et al., 2013, preprint (arXiv:1303.5062)
 Bhat N. D. R., Cordes J. M., Camilo F., Nice D. J., Lorimer D. R., 2004, *ApJ*, 605, 759
 Burke-Spolaor S., Bailes M., Ekers R., Macquart J.-P., Crawford F., III, 2011, *ApJ*, 727, 18
 Cordes J. M., Lazio T. J. W., 2002, preprint (astro-ph/0207156)
 Cordes J. M., McLaughlin M. A., 2003, *ApJ*, 596, 1142
 de Blok E. W. J. G., Booth R., Jonas J., Fanaroff B., 2010, *Proceedings of the ISKAF2010 Science Meeting*, available at: <http://pos.sissa.it/cgi-bin/reader/conf.cgi?confid=112>, p. 5
 Dewdney P. E., Turner W., Millenaar R., McCool R., Lazio J., Cornwell T. J., 2013, SKA-TEL-SKO-DD-001
 Ellingson S. W., Clarke T. E., Cohen A., Craig J., Kassim N. E., Pihlstrom Y., Rickard L. J., Taylor G. B., 2009, *IEEE Proc.*, 97, 1421
 Fong W. et al., 2012, *ApJ*, 756, 189
 Gehrels N., 1986, *ApJ*, 303, 336
 Green A., Madsen G. J., Campbell-Wilson D., Thakkar D., Banyer J., Hunstead R. W., 2012, *Proceedings of the Meeting, Resolving The Sky – Radio Interferometry: Past, Present and Future*, available at: <http://pos.sissa.it/cgi-bin/reader/conf.cgi?confid=163>

- Hankins T. H., Rickett B. J., 1975, *Methods Comput. Phys.*, 14, 55
- Ioka K., 2003, *ApJ*, 598, L79
- Johnston S., Feain I. J., Gupta N., 2009, in Saikia D. J., Green D. A., Gupta Y., Venturi T., eds, *ASP Conf. Ser. Vol. 407, The Low-Frequency Radio Universe*. Astron. Soc. Pac., San Francisco, p. 446
- Keane E. F., McLaughlin M. A., 2011, *Bull. Astron. Soc. India*, 39, 333
- Keane E. F., Kramer M., Lyne A. G., Stappers B. W., McLaughlin M. A., 2011, *MNRAS*, 415, 3065
- Keane E. F., Stappers B. W., Kramer M., Lyne A. G., 2012, *MNRAS*, 425, L71
- Keith M. J. et al., 2010, *MNRAS*, 409, 619
- Large M. L., Vaughan A. E., 1971, *MNRAS*, 151, 277
- Law C. J., Jones G., Backer D. C., Barott W. C., Bower G. C., Gutierrez-Kraybill C., Williams P. K. G., Werthimer D., 2011, *ApJ*, 742, 12
- Li W., Chornock R., Leaman J., Filippenko A. V., Poznanski D., Wang X., Ganeshalingam M., Mannucci F., 2011, *MNRAS*, 412, 1473
- Lorimer D. R., Bailes M., McLaughlin M. A., Narkevic D. J., Crawford F., 2007, *Sci*, 318, 777
- Lorimer D. R., Karastergiou A., McLaughlin M. A., Johnston S., 2013, *MNRAS*, preprint (arXiv:1307.1200)
- Manchester R. N. et al., 2001, *MNRAS*, 328, 17
- Manchester R. N., Fan G., Lyne A. G., Kaspi V. M., Crawford F., 2006, *ApJ*, 649, 235
- Narayan R., 1992, *R. Soc. Lond. Philos. Trans. Ser. A*, 341, 151
- Phillips M. M., 1993, *ApJ*, 413, L105
- Rickett B. J., 1990, *ARA&A*, 28, 561
- Stappers B. W. et al., 2011, *A&A*, 530, A80
- Staveley-Smith L., Wilson W. E., Bird T. S., Sinclair M. W., Ekers R. D., Webster R. L., 1995, in Emerson D. T., Payne J. M., eds, *ASP Conf. Ser. Vol. 75, Multi-Feed Systems for Radio Telescopes*. Astron. Soc. Pac., San Francisco, p. 136
- Thornton D. et al., 2013, *Sci*, 341, 53
- Tingay S. J. et al., 2013, *Publ. Astron. Soc. Aust.*, 30, 7
- van Haarlem M. P. et al., 2013, *A&A*, 556, A2
- Wright E. L., 2006, *PASP*, 118, 1711

APPENDIX A: TABLES OF DERIVED RATES

Here we tabulate the results of our simulations. Table A1 shows the number of FRBs expected per hour in our simulations of beamformed observations, and Table A2 shows the number of FRBs expected per hour from our simulations of imaging observations. In each table, the rates are given for both the no-scattering and the high-scattering simulations.

Table A1. Derived rates for the numbers of FRBs in no-scattering/high-scattering simulations of beamformed observations.

Instrument	FRBs/hour derived from no-scattering/high-scattering simulations				
	$\alpha = 0$	$\alpha = -1$	$\alpha = -2$	$\alpha = -3$	$\alpha = -4$
SKA-low	0.35/0.021	0.35/0.045	0.35/0.11	0.35/0.26	0.35/0.66
SKA ₁ -low	0.35/0.01	0.35/0.023	0.35/0.056	0.35/0.14	0.35/0.38
SKA-mid	0.0064/0.007	0.0064/0.0085	0.0064/0.01	0.0064/0.013	0.0064/0.018
SKA ₁ -mid	0.0064/0.0042	0.0064/0.0049	0.0064/0.0059	0.0064/0.0075	0.0064/0.01
LOFAR-HBA	0.2/0.0018	1.9/0.01	1.9/0.036	1.9/0.13	1.9/0.45
LOFAR-LBA	0.00012/5.8e-06	0.012/4.6e-05	1.3/0.00036	1.3/0.0028	1.3/0.024
MWA	0.19/0.0037	2.6/0.018	2.6/0.056	2.6/0.17	2.6/0.5
ASKAP	0.23/0.025	0.38/0.037	0.38/0.058	0.38/0.084	0.38/0.13
MeerKAT	0.011/0.0042	0.011/0.0049	0.011/0.006	0.011/0.0073	0.011/0.0092
Parkes	0.014/0.0021	0.014/0.0026	0.014/0.0033	0.014/0.004	0.014/0.0054
UTR-2	6.3e-06/2.3e-06	0.00069/2.3e-06	0.51/2.3e-06	0.51/0.00014	0.51/0.0028
Molonglo	0.15/0.011	0.15/0.017	0.15/0.026	0.15/0.042	0.15/0.066
LWA	0.0074/1.1e-05	0.31/8.6e-05	0.31/0.0013	0.31/0.0078	0.31/0.046

Table A2. Derived rates for the numbers of FRBs in no-scattering/high-scattering simulations of imaging observations.

Instrument	FRBs/hour derived from no-scattering/high-scattering simulations				
	$\alpha = 0$	$\alpha = -1$	$\alpha = -2$	$\alpha = -3$	$\alpha = -4$
SKA-low	0.012/0.056	0.35/0.22	0.35/0.69	0.35/1.5	0.35/3.0
SKA ₁ -low	0.0019/0.015	0.032/0.08	0.35/0.38	0.35/0.98	0.35/2.2
SKA-mid	0.0064/0.014	0.0064/0.02	0.0064/0.034	0.0064/0.05	0.0064/0.062
SKA ₁ -mid	0.0017/0.0063	0.0064/0.009	0.0064/0.014	0.0064/0.027	0.0064/0.048
LOFAR-HBA	0.00043/0.0028	0.0075/0.03	1.9/0.2	1.9/1.4	1.9/4.3
LOFAR-LBA	6e-07/5.8e-06	4.7e-06/4.6e-05	0.00019/0.0012	1.3/0.055	1.3/0.51
MWA	0.00025/0.0024	0.0041/0.028	0.19/0.2	2.6/1.3	2.6/5.2
ASKAP	0.00086/0.0084	0.0024/0.023	0.0097/0.066	0.38/0.17	0.38/0.49
MeerKAT	0.00047/0.004	0.001/0.0057	0.011/0.009	0.011/0.016	0.011/0.037
Parkes	–	–	–	–	–
UTR-2	2.4e-07/2.3e-06	2.4e-07/2.3e-06	0.00016/0.00048	0.51/0.011	0.51/0.11
Molonglo	0.001/0.01	0.005/0.023	0.15/0.046	0.15/0.1	0.15/0.32
LWA	1.1e-06/1.1e-05	9.6e-05/0.00066	0.029/0.015	0.31/0.12	0.31/0.52